

Supporting Information

In-situ Growing MoS₂ Nanosheets Array and TS₂ (T=Fe, Co, Ni) Nanocubes onto Molybdate for Efficient Oxygen Evolution Reaction and Improved Hydrogen Evolution Reaction

Jianghao Wang,^a Liping Li,^b Liping Wang,^b Yifeng Liu,^b Wengang Sun,^b Wenwen Li^b
and Guangshe Li*^{a,b}

- a. Key Laboratory of Design and Assembly of Functional Nanostructures, Fujian Institute of Research on the Structure of Matter, Chinese Academy of Sciences, Fuzhou 350002, P.R. China
- b. State Key Laboratory of Inorganic Synthesis & Preparative Chemistry, College of Chemistry, Jilin University, Changchun 130012, P.R. China

Contents

Figure S1. XRD patterns of FCNMS synthesized when using different amounts of L-cys.	3
Figure S2. SEM images of FCNMS synthesized using different dosage of L-cys.	4
Figure S3. XRD patterns of various molybdate samples.	5
Figure S4. Pore size distribution curves.	6
Figure S5. SEM images for the as-prepared samples.	7
Figure S6. TEM and HRTEM images for NCMS and NFMS.	8
Figure S7. STEM and corresponding EDX element of FCNMS.	9
Figure S8. Elemental mapping images for NCMS and NFMS.	10
Figure S9. TEM and HRTEM images for NCMO and NFMO.	11
Figure S10. TEM and HRTEM images for CMO and NMO.	12
Figure S11. Linear combination fitting result of Mo K-edge.	13
Figure S12. EDLC for samples.	14
Figure S13. Equivalent electric circuit of the cell.	14
Table S1. EIS fitting results of the components of the circuit.	15
Figure S14. Polarization curves of FCNMS samples with various mass loading.	16
Figure S15. Polarization curves and Tafel plots of NCMS and NFMS for OER.	17
Figure S16. OER performance comparison of this work with previous researches. .	18
References.	19

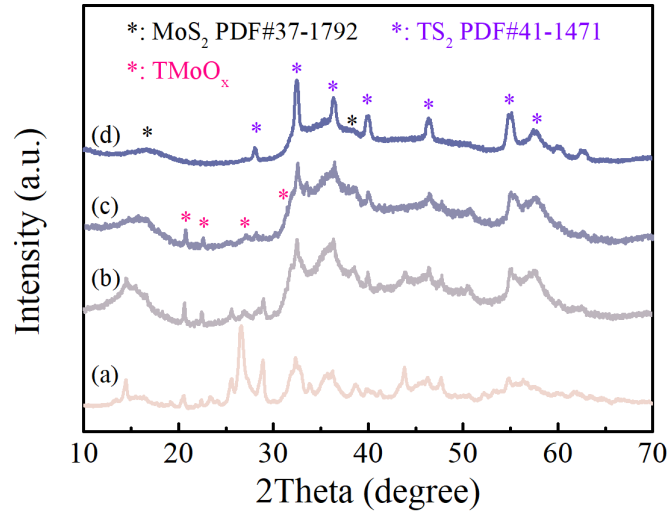


Figure S1. XRD patterns of FCNMS synthesized when using different amounts of L-cys: (a) 0.12 g; (b) 0.24 g; (c) 0.36 g and (d) 0.48 g.

As shown in Figure S1, with an increase in sulfidizer dosage, the characteristic XRD peaks of molybdate became weak gradually, whereas the XRD peaks for CoS₂ became strong. When 0.48g L-cys was used, all the molybdate peaks disappeared. All these observations demonstrate that sulfidizer dosage plays a key role in preparing the hierarchical nanostructure.

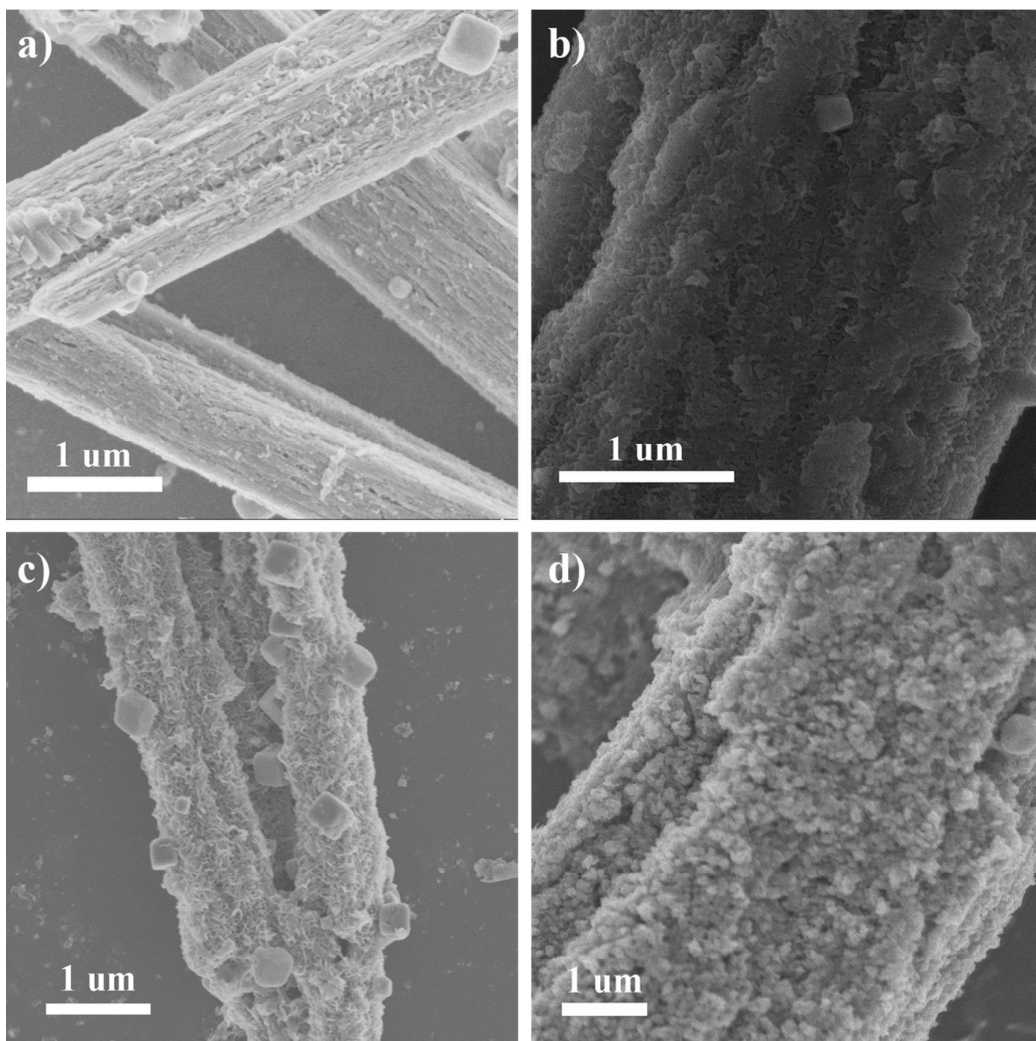


Figure S2. SEM images of FCNMS synthesized using different dosage of L-cys: (a) 0.12g; (b) 0.24g; (c) 0.36g and (d) 0.48g.

As shown in Figure S2, with an increase in sulfidizer dosage, more and more nanosheets of MoS_2 and nanocubes of TS_2 were grown onto the surface of FCNMO nanorods. Because not too much of nanosheet array were formed for FCNMS when using lower concentrations of L-cys (e.g., the cases of adding 0.12 and 0.24g), we chose the addition amount of 0.36 g L-cys in the subsequent synthesis of our samples.

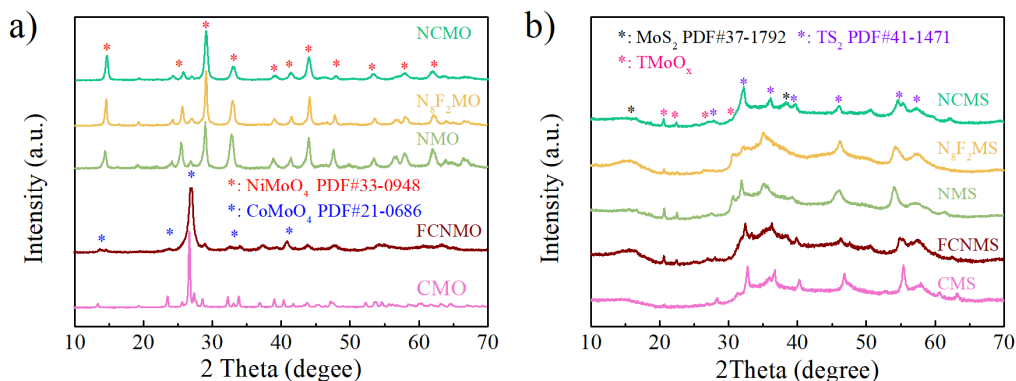


Figure S3. XRD patterns of various molybdate samples: (a) before and (b) after sulfide.

As shown in Figure S3a, the diffraction peaks of CMO and FCNMO could be well indexed in terms of the standard data for CoMoO₄ (JPCDS, No. 21-0868), while the diffraction patterns of NMO, NCMO, and NFMO matched well the data for NiMoO₄ (JPCDS, No. 33-0948), demonstrating that we successfully synthesized the transition metal molybdate samples.¹ CMO and FCNMO exhibited different phase structure from NMO, NCMO, and NFMO, which might be related to the stability of transition metal molybdate. Usually, beta-CoMoO₄ is stable at room temperature, whereas NiMoO₄ is unstable.^{2,3} The strongest peak for FCNMO located at two theta ca. 27° is ascribed to the plane (0 0 2) of cobalt molybdate. XRD patterns of sulfured samples CMS, NMS, NCMS, NFMS and FCNMS are shown in Figure S3b. The peaks at two theta of 27.8°, 32.3°, 36.2°, 39.9° 46.3° and 54.9° are attributed to the diffractions of TS₂ (JPCDS, No. 41-1471), while the diffraction peak at two theta of 14.8° corresponds to the (0 0 2) plane of the hexagonal MoS₂ (JPCDS, No. 75-1539).

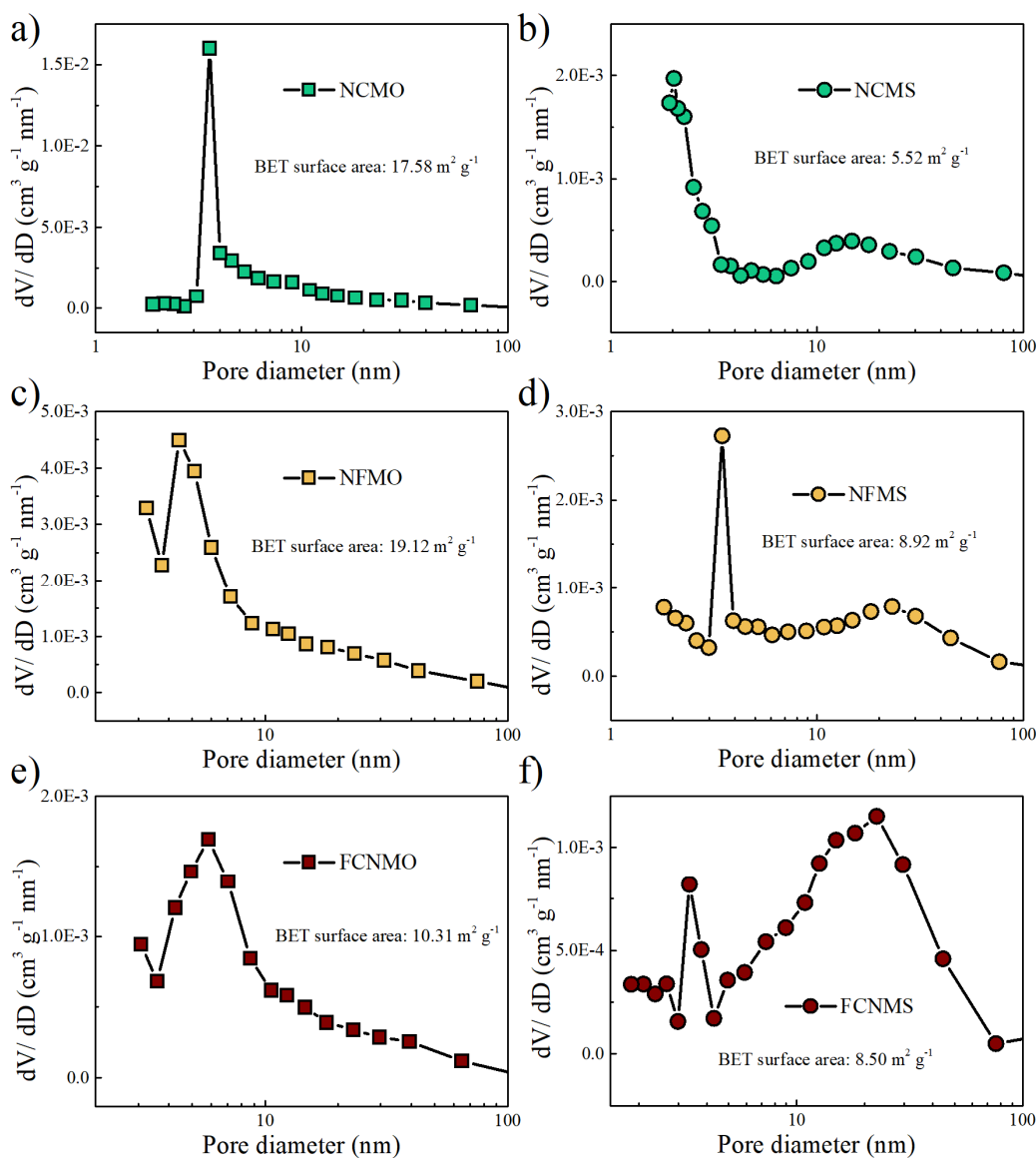


Figure S4. Pore size distribution curves of molybdate samples before and after sulfide: (a), (c) and (e) for un-sulfide samples NCMO, NFMO and FCNMO, and (b), (d) and (f) for sulfide samples NCMS, NFMS and FCNMS, accordingly.

As shown in Figure S4, the presence of mesopores with dimension of ca. 4 nm and 20 nm after sulfuration was verified using BJH formula. The mesopores size observed for our samples were similar to previously reported values of 4 and 10 nm, confirming the formation of porous nanostructures.⁴ The smaller surface areas of FCNMS, NFMS, and NCMS indicate the improved catalytic activity after sulfidation cannot attribute to BET surface

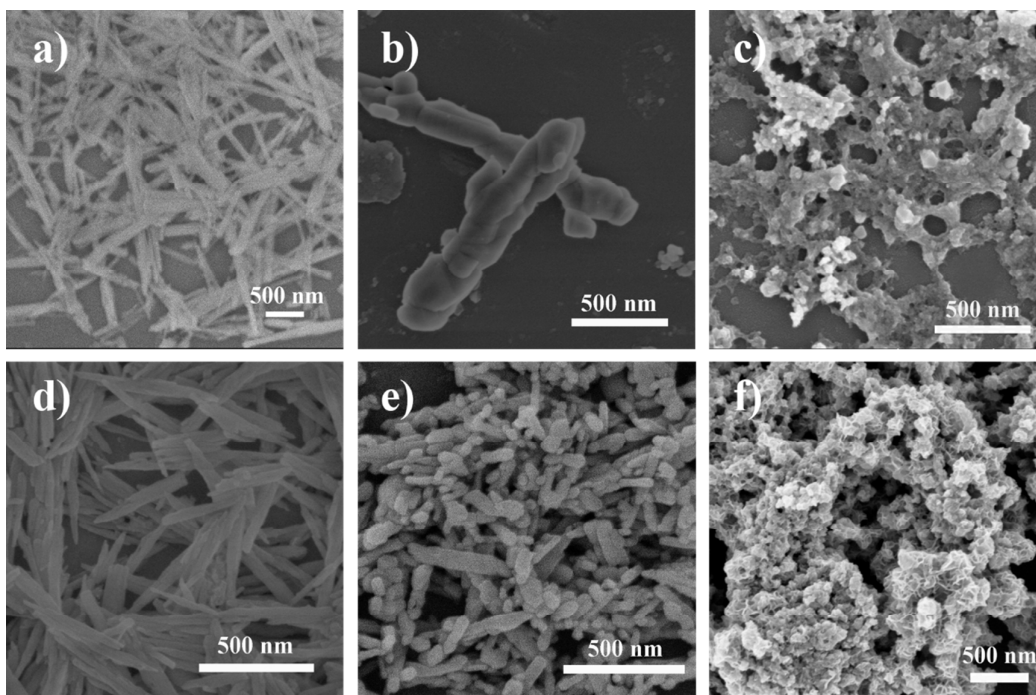


Figure S5. SEM images for the as-prepared materials. (a) CMH, (b) CMO, (c) CMS, (d) NMH, (e) NMO, and (f) NMS.

As shown in Figure S5, CMO and NMO can keep rod morphology after calcination, whereas CMS and NMS cannot keep rod-like morphology after sulfidation.

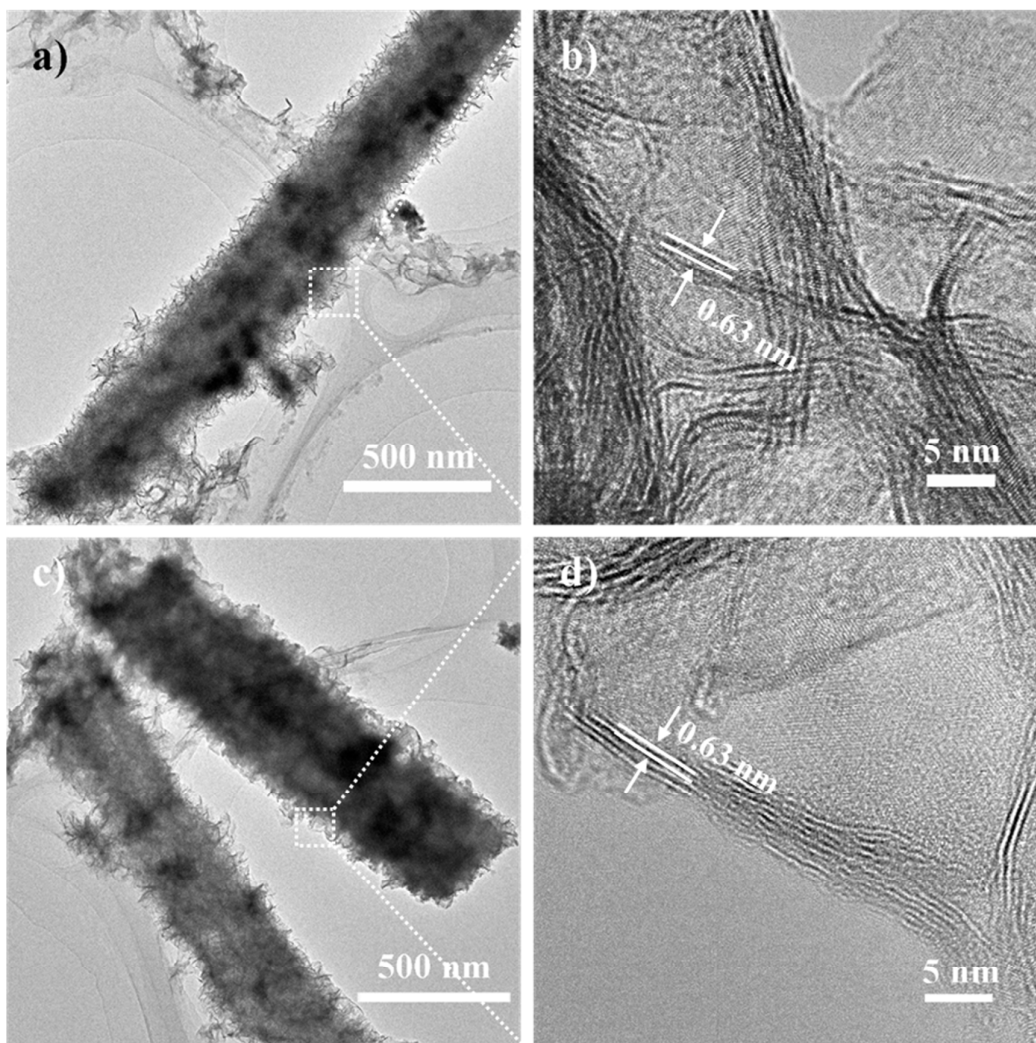


Figure S6. TEM and HRTEM images for samples. (a) and (b) NCMS, (c) and (d) NFMS.

As shown in Figure S6, TEM and HRTEM images for NCMS and NFMS were similar to FCNMS results. TEM analysis in Figures S6 (a, c) demonstrates the hierarchical structure characteristic of NCMS and NFMS, consistent with the observations by SEM (Figure 2).

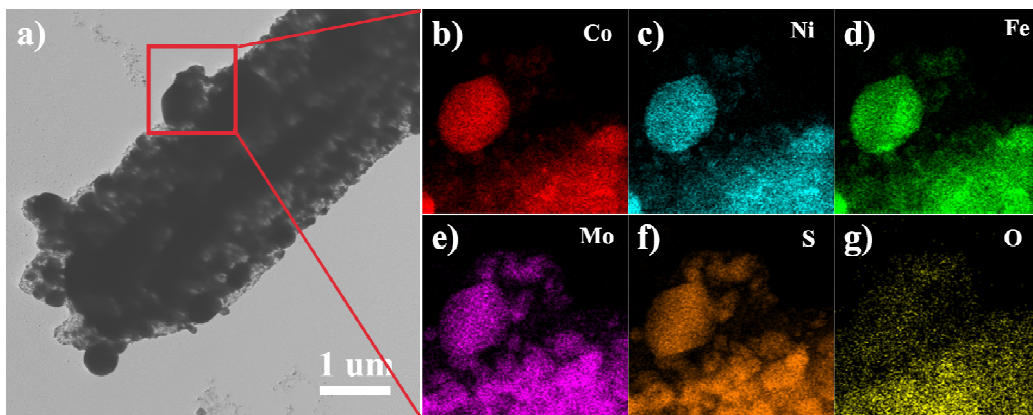


Figure S7. STEM and corresponding EDX element mapping of FCNMS sample: (a) STEM image, (b) Co (Red), (c) Ni (cyan), (d) Fe (green), (e) Mo (purple), (f) S (orange) and (g) O (yellow).

Figure S7 shows STEM and corresponding EDX element mapping images of isolated nanocube on the surface of FCNMS. As shown in Figure S7, Co, Ni, Fe, and S are dispersed uniformly in nanocube as we expected, which directly prove the composition of TS_2 . In addition, we can also find Mo is dispersed in nanocube, which may attribute to the epitaxial growth of MoS_2 on the surface of TS_2 as previously reported.⁵

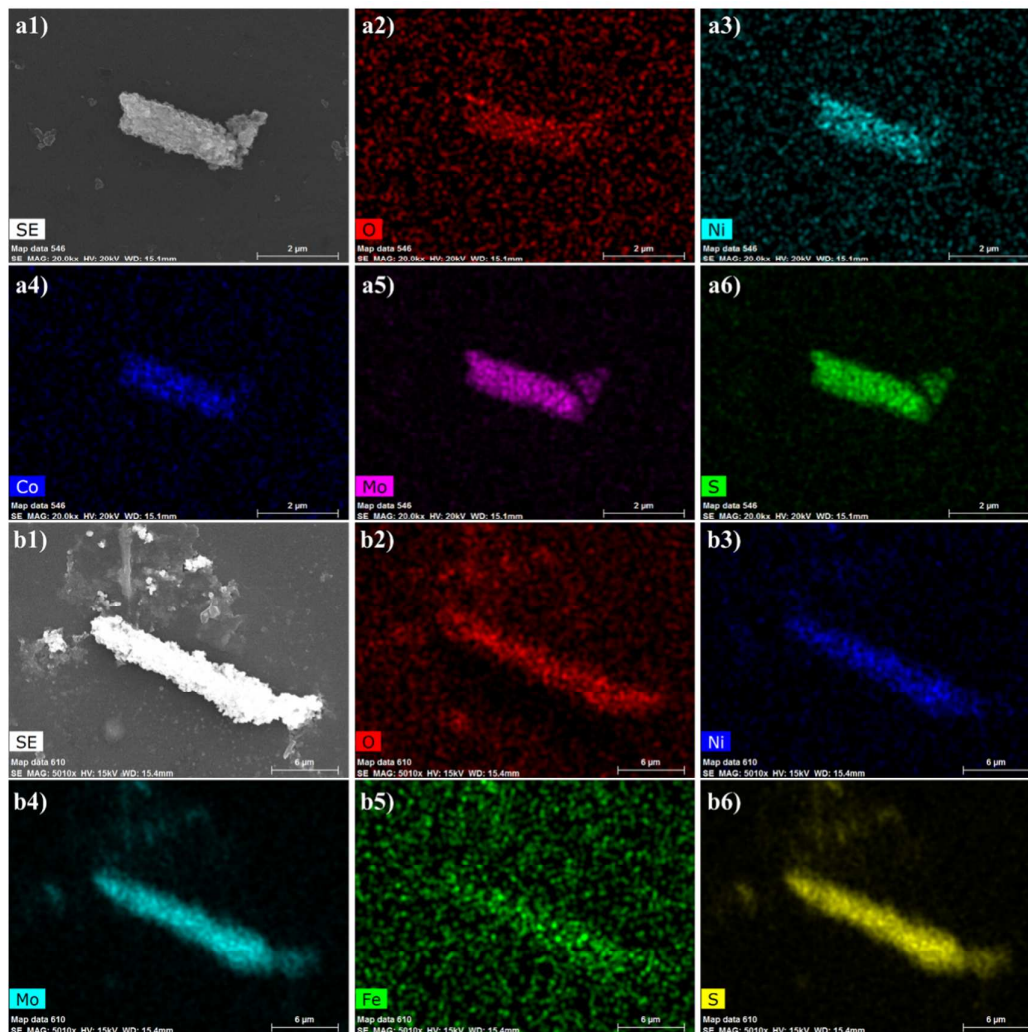


Figure S8. Elemental mapping images for samples. a1)-a6) NCMS, and b1)-b6) NFMS.

As shown in Figure S8, Co, Ni, Mo, O, S and Ni, Fe, Mo, O, S were uniformly dispersed on nanorods of NCMS and NFMS, respectively. This result was similar to FCNMS (Figure 4).

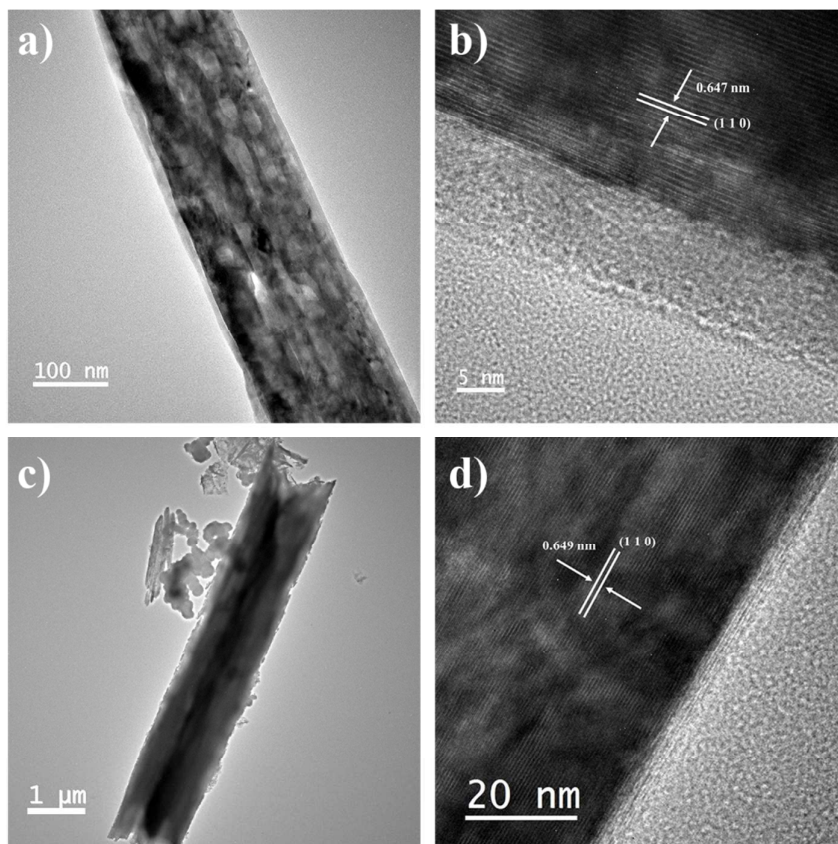


Figure S9. TEM and HRTEM images of the samples: (a, b) NCMO, and (c, d) NFMO.

Figure S9 shows the TEM and HRTEM images for NCMO and NFMO. TEM analysis in Figures S9 (a, c) demonstrates the rod characteristic of NCMO and NFMO, consistent with the observations by SEM (Figure 2). As shown in Figure S9 (b, d), the lattice distances of NCMO and NFMO were 0.65 nm (Figure S9), closer to 0.62 nm for the plane (1 1 0) of NiMoO_4 (PDF# 33-0948).

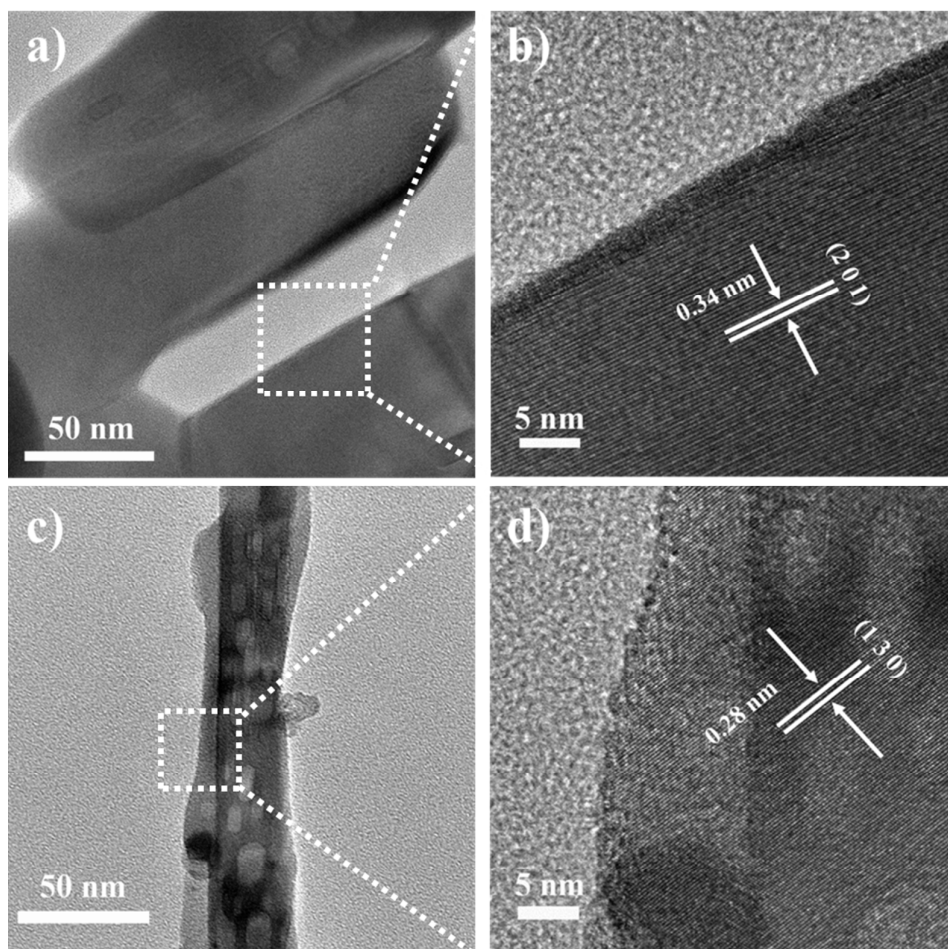


Figure S10. TEM and HRTEM images of the samples: (a, b) CMO, and (c, d) NMO.

Figure S10 shows the TEM and HRTEM images for CMO and NMO. As shown in Figure S10 (b, d), the lattice spacing of CMO and NMO were 0.34 and 0.28 nm, respectively, which could be assigned to the planes (201) and (130).

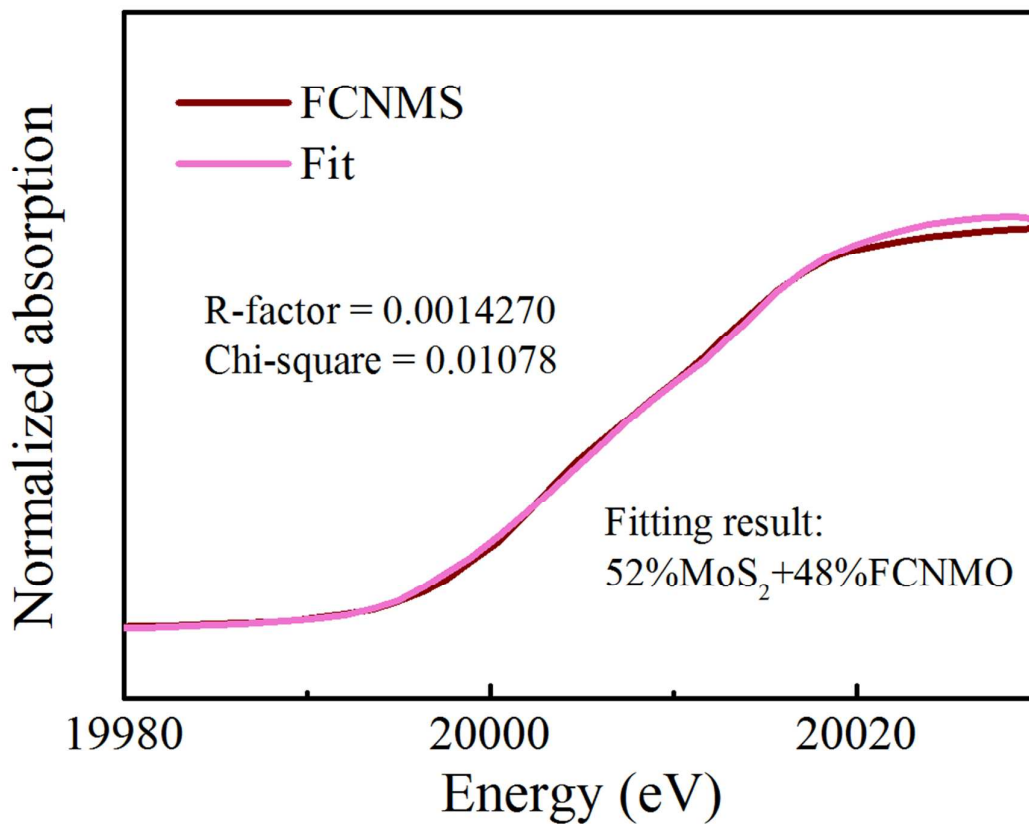


Figure S11. Linear combination fitting result of Mo K-edge XANES for the sample FCNMS.

To examine the valence states of Mo ions and composition in FCNMS, their XANES data were processed according to the standard procedures using ATHENA module implemented in the IFEFFIT software packages. The fitting result was shown in Figure S11, where about 52 % Mo⁶⁺ ions were reduced to Mo⁴⁺.

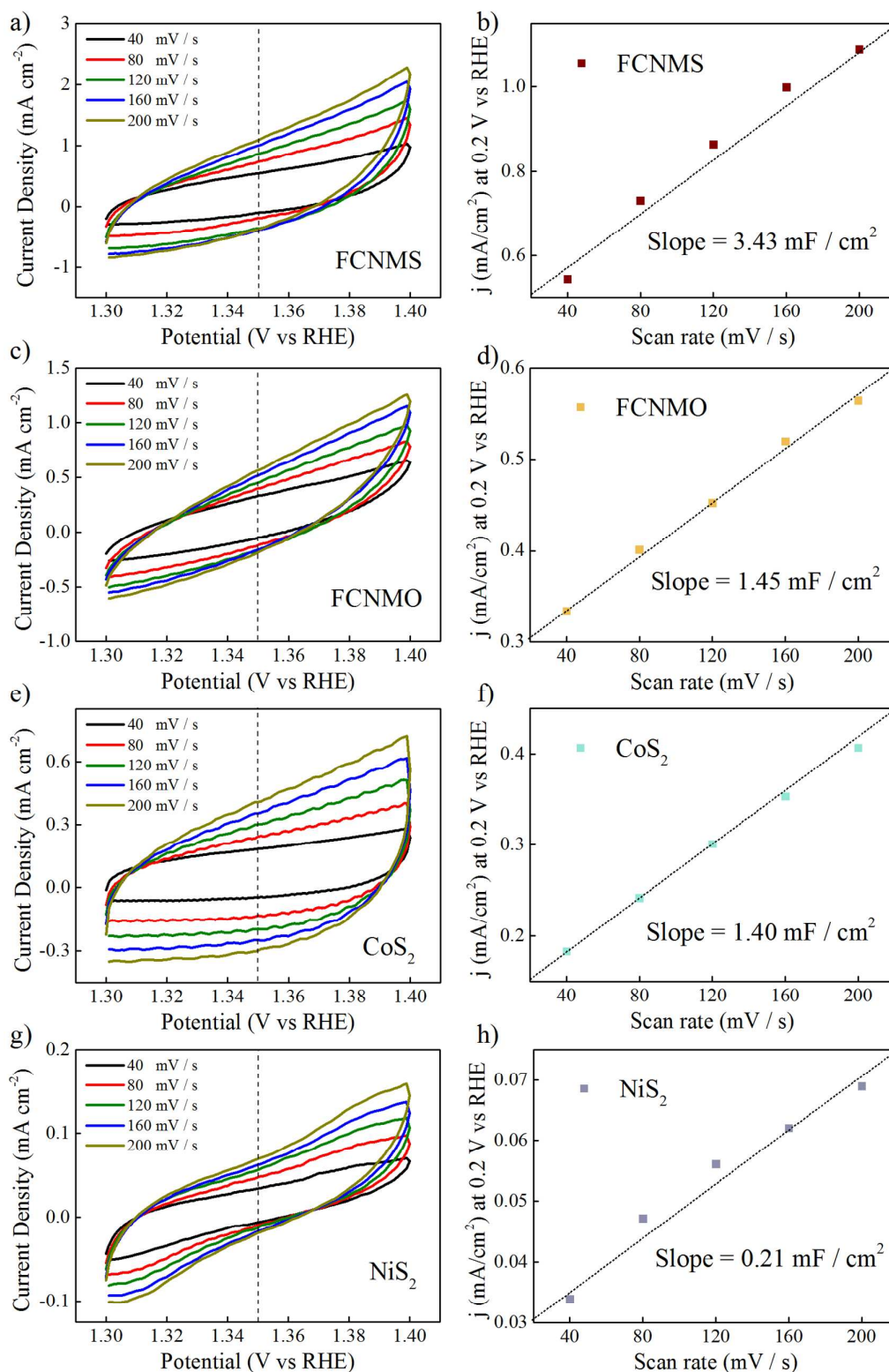


Figure S12. a), c), e) and g): electrochemical double layer capacitance curves for FCNMS, FCNMO, CoS₂, and NiS₂ with different scan rates; b), d), f) and h): plots of current densities at 1.35 V (vs RHE) versus scan rates of these samples.

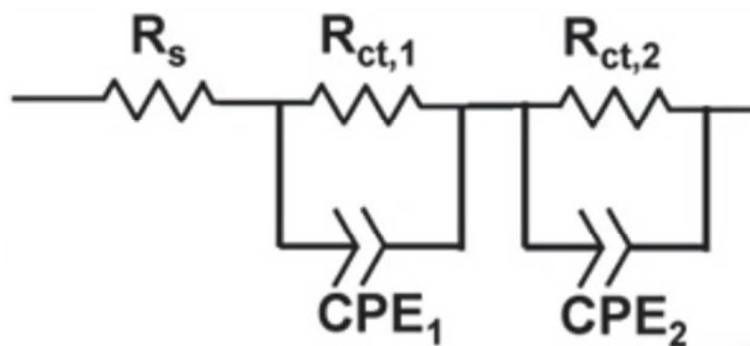


Figure S13. Equivalent electric circuit of the cell.

Table S1. EIS fitting results of the components of the circuit shown in Figure 7c

Samples	$R_s(\Omega)$	$R_{ct,1}(\Omega)$	CPE_{1-p}	$R_{ct,2}(\Omega)$	CPE_{2-p}
FCNMS	5.11	2.907	0.71	6.09	0.78
FCNMO	5.44	0.17	1.10	17.29	0.75
NiS ₂	4.59	0.21	1.90	736.30	0.87
CoS ₂	5.05	0.34	1.14	24.12	0.80
IrO ₂	5.55	0.39	1.14	8.91	0.81

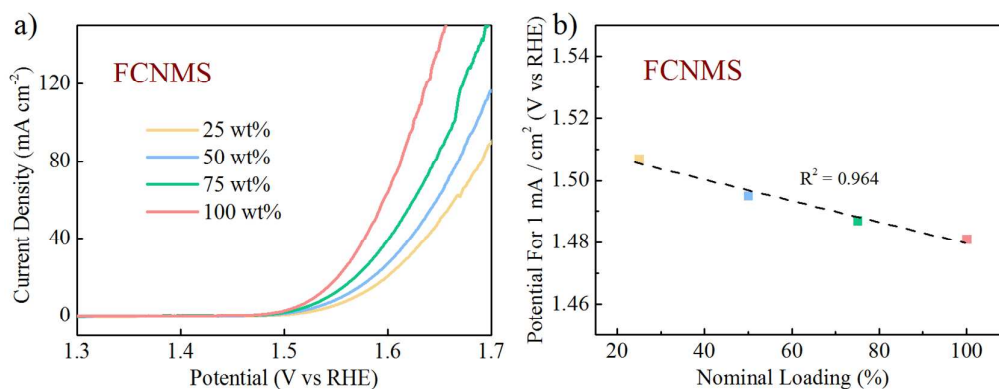


Figure S14. (a) Polarization curves of FCNMS samples with 25%, 50%, 100% mass loading, and (b) linear variation of potential vs. nominal mass loading.

Polarization curves of different catalyst loadings (from 25% to 100%) of FCNMS are shown in Figure S14. To minimize the effect of iR -correction on the apparent activity, the potential at 1 mA cm⁻² is usually used to be a metric for comparing the catalytic activities. As shown in Figure S14b, the catalytic activities rose linearly with catalyst loading, demonstrating that the measured activities were in the regime of intrinsic kinetics.

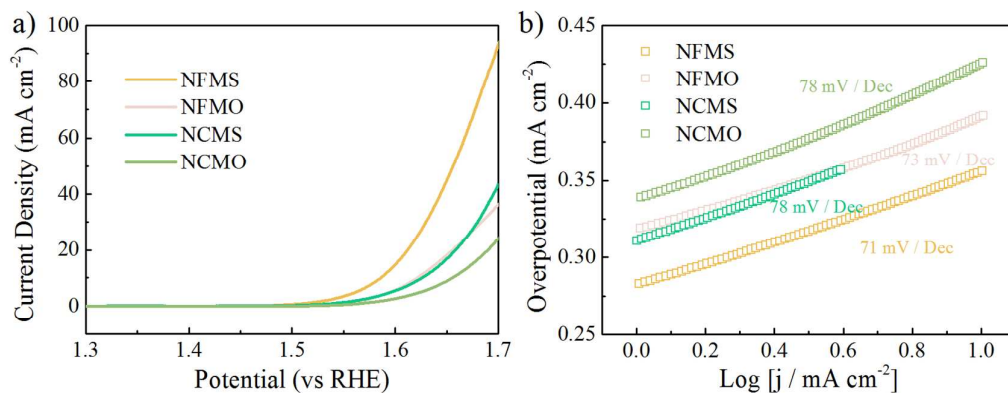


Figure S15. (a) Polarization curves of NCMS and NFMS for OER, and (b) Corresponding Tafel plots derived from (a).

Figure S15 shows polarization curves and corresponding Tafel plots of NCMS, NCMO, NFMS, and NFMO for OER. As shown in Figure S15a, NFMS and NCMS achieved a current density of 10 mA cm⁻² at 1.56 V and 1.62 V, respectively, which were apparently superior to NCMO and NFMO. Furthermore, the resulting Tafel slope of the NCMS and NFMS were 71 and 78 mV Dec⁻¹, respectively.

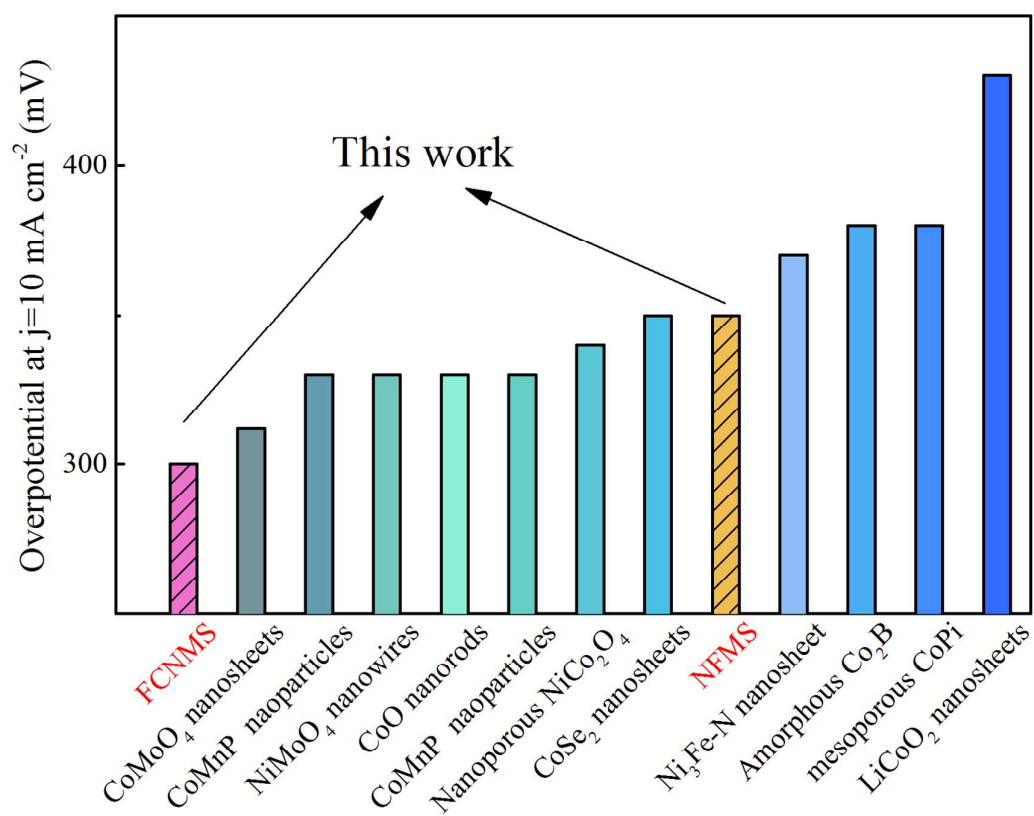


Figure S16. OER overpotentials of the FCNMS, NFMS and the ever reported electrocatalysts for comparison at 10 mA cm^{-2} in 1 M KOH.

- (1) Brito, J. L.; Barbosa, A. L. Effect of Phase Composition of the Oxidic Precursor on the HDS Activity of the Sulfided Molybdates of Fe(II), Co(II), and Ni(II). *J. Catal.* **1997**, *171* (2), 467–475.
- (2) Robertson, L. C.; Gaudon, M.; Jobic, S.; Deniard, P.; Demourgues, A. Investigation of the First-Order Phase Transition in the $\text{Co}_{1-x}\text{Mg}_x\text{MoO}_4$ Solid Solution and Discussion of the Associated Thermochromic Behavior. *Inorg. Chem.* **2011**, *50* (7), 2878–2884.
- (3) Rodriguez, J. A.; Chaturvedi, S.; Hanson, J. C.; Albornoz, A.; Brito, J. L. Electronic Properties and Phase Transformations in CoMoO_4 and NiMoO_4 : XANES and Time-Resolved Synchrotron XRD Studies. *J. Phys. Chem. B* **1998**, *102* (8), 1347–1355.
- (4) Wang, J.; Wang, W.; Wang, Z.; Chen, J. G.; Liu, C. Porous MS_2/MO_2 (M = W, Mo) Nanorods as Efficient Hydrogen Evolution Reaction Catalysts. *ACS Catal.* **2016**, *6* (10), 6585–6590.
- (5) Zhang, H.; Li, Y.; Xu, T.; Wang, J.; Huo, Z.; Wan, P.; Sun, X. Amorphous Co-Doped MoS_2 Nanosheet Coated Metallic CoS_2 Nanocubes as an Excellent Electrocatalyst for Hydrogen Evolution. *J. Mater. Chem. A* **2015**, *3* (29), 15020–15023.